

Thermal Behavior of Biomass under Thermochemical Treatment at Different Air Fluxes in an Updraft Reactor

Kittipass Wasinaron,^a Sarawut Sungworagarn,^b Prasan Sathitruangsak,^b Wichean Singmai,^c and Kasemsil Onthong^{c,*}

Thermochemical treatment was investigated experimentally at different air fluxes in an updraft reactor. The test rig was equipped with a special attached door that will open at a specific time step. This unique feature allows investigators to obtain information on the packed bed color variation along the different heights of the reactor that evolves at different points in time. The analysis focused on the temperature dynamics obtained from installed thermocouples with the packed bed color variation at each time step. The investigation was conducted for three different supply air mass fluxes, which were 670, 480, and 190 kg/m²h. The general thermal behavior is addressed in the first part of the paper because it is similar for all different input air mass fluxes. Next, the distinctive operation parameters among different air mass fluxes are discussed; these included the hot spot zone, fuel conversion characteristic, temperature distribution, heat transfer, and kinetic activities along the height of the reactor.

DOI: 10.15376/biores.18.2.3452-3470

Keywords: Biomass; Gasification; Updraft; Packed bed; Pyrolysis; Volatile combustion

Contact information: a: School of International and Interdisciplinary Engineering Programs, School of Engineering, King Mongkut's Institute of Technology Ladkrabang, 1 Chalong Krung 1 Alley, Lat krabang, Bangkok 10520, Thailand; b: Department of Mechanical Engineering, School of Engineering and Industrial Technology, Mahanakorn University of Technology 140 Cheum-Sampan Road, Nong-Chok, Bangkok 10530, Thailand; c: Department of Teacher Training in Mechanical Engineering, King Mongkut's University of Technology North Bangkok, 1518 Phacharat 1 Road, Bangsue, Bangkok 10800, Thailand; *Corresponding author: kasemsil.o@fte.kmutnb.ac.th

INTRODUCTION

Thailand is an agricultural country that has several types of agricultural waste distributed over the country area. These wastes can be used as an alternative fuel to provide heat, thus lowering the amount of energy imports. There are two ways to generate heat from biomass, which are thermochemical and digestion systems. In thermochemical systems, heat is generated by the oxidation of the fuel with oxygen. For digestion systems, the biomass is broken down by bacteria in the absence of oxygen to produce biogas, which later burns to provide heat.

There are many fixed bed updraft thermochemical treatment applications. For example, there are biomass updraft gasification, grate firing boilers, and incinerator combustion (Shin and Choi 2000). They operate by passing the air upward through the packed fuel bed. The fixed bed updraft thermochemical treatment under constant air mass flux may undergo different modes (gasification, char gasification, and combustion) during the different instants along the process (Kim *et al.* 2016). This is due to the dynamics of several parameters (bed height, oxidation, combustion front location, and reduction layer width) being continuously altered along the process. Ryu *et al.* (2006) experimentally investigated the combustion of different biomass materials in a fixed bed. The described system operates with the overfired updraft-packed bed configuration, in which the flame is ignited at the top surface of the bed. After ignition, the flame front is propagated down

through the bed in a counter-current direction with the supply air. After the front reaches the bottom, the process is changed to char gasification mode, in which the flame propagation is altered to a co-current direction. For pinewood particles sized 20 mm and the airflow of 160 l/min, it was found that the CO and CO₂ concentrations were around 15% during the downward front propagation phase. Then, during the char gasification phase, CO concentration was raised to 23%. In the short period before the flame was extinguished, the CO₂ was raised to 19%, while CO production was reduced to zero, implying that the combustion process has dominant. The overfired updraft packed bed process evolutions resemble the grate-firing combustor, in which the finite height of packed fuel particles is located on the grate (Rashidian *et al.* 2016). The ignition is taking place at the top surface of the bed. The secondary air is injected above the bed surface to allow combustible gas combustion over the freeboard area.

Thermochemical treatment in packed-bed can be divided into combustion systems and gasification systems. Packed-bed combustion systems can be explained by a three-step model (Friberg and Blasiak 2002). The process starts with the conversion system, where the combustible off-gas is generated by thermochemical treatment of the packed bed. The second unit is the combustion system, in which secondary air is injected to allow gas phase combustion. The third unit is the heat exchanger. In packed bed gasification, the combustible gas is produced from the gasification reactor and will route to the burner or the heat engine where the combustion heat release will be taking place. The air or gasification medium is passed through the homogeneous packed fuel bed either from the top (downdraft) or underneath (updraft).

During thermochemical treatment in the fixed bed, there is the evolution of different processes along the height of the packed bed, including pyrolysis combustion, char reduction, and drying. The kinetic inside the reactor is comprised of the homogeneous reaction (gas phase reaction) inside the pore space of the packed bed and the heterogeneous reaction which takes place at the surface area of the fuel. The convection heat transfer along the bed is driven by the difference in temperature of the flowing gas inside the pore space and the fuel particles at the specific location. The radiation heat transfer of the flowing gas can be ignored, while the Rosseland radiation model can be used to estimate radiation heat transfer between solid fuel particles inside the packed bed which is proportional to the local temperature gradient (Voss *et al.* 2013). The heat transfer inside the packed bed resembles the submerged flame of the combustion inside the porous inert media (Wasinarom *et al.* 2019, 2021).

To improve fixed-bed thermochemical treatment processes operating in gasification or combustion systems, an understanding of physical phenomena occurring within the packed beds is required. Combustion behaviors of solid fuel on packed beds have been studied by a number of researchers. Yang *et al.* (2005) studied the fuel size effect on pinewood combustion in a packed bed. Ryu *et al.* (2007) revealed that the packed bed combustion of textile residual can be improved by mixing the textile residual with the cardboard. Jancauskas and Buineviccius (2021) studied the flue gas recirculation ratio and excess air effect on flue gas emission in a grate-firing biofuel boiler. Varunkumar *et al.* (2013) investigated flame propagation in packed bed biomass.

There have been many studies examining the influence of several parameters of packed bed gasification. Susastriawan *et al.* (2018) have studied the effect of tuyer distance on the delivered gas composition. They concluded that the tuyer distance has an effect on the producer gas composition. Increasing the tuyer distance above the grate will allow more mole fraction of CH₄, CO, and H₂, which considerably improves the HHV (Higher Heating Value) in the producer gas. Mehta and Richards (2017) have studied the performance of a TLUD (Top-Lit Updraft) gasification stove. They found that the producer gas energy content was maximized at the superficial velocity of 9 cm/s. Susastriawan *et al.* (2021) optimized the bluff body configuration and studied the impact of feedstock type in an

updraft gasification stove.

Mathematical models can serve as a tool to gain insight into the thermochemical treatment process of the packed bed. Computational Fluid Dynamics (CFD) modeling is capable of providing detail of the transport phenomena inside the packed bed. The modeler can achieve a trade-off between the level of modeling complication and the effort needed in modeling activities. Some modeling details can be simplified without a major effect on the key process parameters. Many one-dimensional CFD codes were developed (Blasi 2000; Yang *et al.* 2005; Tanui *et al.* 2018). Most of them treated the packed bed domain as a porous media. The phenomena inside the packed bed were simplified by the void fraction concept. The energy conservation equation in the solid domain and fluid domain inside the packed bed were separately solved. The heat transfer between the flowing gas in the pore space and the solid fuel bed was taken into account *via* a source term.

In this paper, the experimental investigation of thermochemical treatment at different air fluxes in an updraft reactor has been performed. The analysis is focused on the temperature dynamics with the packed bed color variation along the different heights of the reactor that evolves at different time steps along the process. The investigation has been conducted for three different supply air mass fluxes. This research allows gasification designers to gain a better insight into updraft thermochemical treatment and increase the ability to analyze

EXPERIMENTAL

Materials

Rice husk was used as a fuel in this work. Its properties and heating values are shown in Table 1 (Madhiyanon *et al.* 2020). The fresh rice husk was baked in a 110 °C temperature controlled oven for 24 h to determine the dry rice husk weight. The moisture content was calculated by the weight difference between the fresh fuel and dry rice husk on a dry basis (Basu 2010). The moisture content was controlled between 6% and 8% in all experiments in this work.

Table 1. Ultimate Analyses of Rice Husk

Ultimate Analysis (% , Dry basis)					Moisture (% , Dry basis)
C	H	O	N	S	6 to 8
38.7	5.1	55.8	0.4	0.04	

Methods

Fixed bed reactor

The reactor tested in this work was comprised of three main parts, which are the air- distributed chamber with the attached fuel grate located underneath, the body of the reactor, and the top cover chamber. All important features of the test rig are shown in Fig. 1. The body of the reactor is made of stainless steel with a diameter of 100 mm and a height of 550 mm. It contains the packed fuel bed during the test. The attached door is designed to allow the investigation of the packed bed color variation along the height at a specific time during the test. The pneumatic agitator is attached to the reactor. It is periodically activated to ensure that the packed bed is settled down homogeneously and prevents cavity forming during the test. The nitrogen purge line is connected to the air distributor chamber under the grate. At the desired point in time, airflow is cut off and nitrogen is made to flow through the bed immediately to ensure that the kinetics inside the reactor are instantly halted. Then, water is sprayed around the reactor surface to allow fast bed cooling. This will reduce the error from the bed pyrolysis, which will continue if the temperature is greater than 300 °C (Reed and Das 1998). The temperature was decreased to below 300 °C

within a minute for every test. The investigator can observe packed bed color variation by opening the attached door. Ten type-K thermocouples are installed along the bed height to measure the temperature distribution in the reactor. The space between each thermocouple is 50 mm. The reactor has an ignition port to ignite the fuel at the lower section. The fuel grate is attached to the reactor body and the air-distributed chamber underneath. It has a grille to support a packed bed inside the reactor while allowing air to flow upward through the bed. The air is supplied to the reactor by the supply air systems. The air volume flow rate is measured by an air rotameter. The temperature is recorded by data logger Yokokawa MW-100 for every 30 seconds interval along the testing period.

Experimental procedure

To operate the test rig, 500 grams of rice husk having the properties as shown in Table 1 are poured into the reactor from the top, which corresponds to the 550 mm height of the packed bed. The airflow rate is regulated by the valve at the rotameter to meet the desired condition in Table 2. Then the ignition port cover is opened and the external burner is placed inside the ignition port to ignite the fuel bed at the grate. During this period, all reading temperatures are monitored by the data logger. If there is any one of the thermocouples that reads over 100 °C, the external burner will be removed and the ignition port will be closed. At the same instant, the stopwatch timer is activated. The data logger is started to record every 30 seconds interval for the entire testing period. The agitator is activated every 2 min during the test. After finished the test, the supply air is cut off. At the same moment, nitrogen is purged through the packed bed from the air-distributed chamber to replace the gas volume inside the reactor. This will ensure the kinetics inside the fuel bed is completely stopped. The cylindrical insulation is removed and the water is sprayed around the reactor surface to cool the bed down to below 50 °C. The attached door is opened to allow the investigator to examine the packed bed color variation along the bed height. Finally, the packed bed residual is removed from the reactor.

The testing procedure is repeated with different testing times at the same air flow rate. Finally, a series of packed bed color evolution along different times at a specific air flow rate can be obtained. The fuel bed color evolution and the temperature distribution data are interpreted to the meaningful physical phenomena along the gasification process.

The equivalence ratio was calculated by the total mass of air flowing through the reactor from the beginning of the test until the peak instant (actual air) divide by the stoichiometric air corresponding to the fuel mass loss during the test (Eq.1) (Basu 2010). The stoichiometric air can be found by the complete combustion equation of the fuel composition in Table 1.

$$\text{Equivalence Ratio} = \frac{\text{Actual air}}{\text{Stoichiometric air}} \quad (1)$$

Table 2. Experimental Condition

Air Flow Rate	Air Mass Flux	Equivalence Ratio (at peak instant)
70 L/min	670 kg/m ² h	0.27
50 L/min	480 kg/m ² h	0.33
20 L/min	190 kg/m ² h	0.20

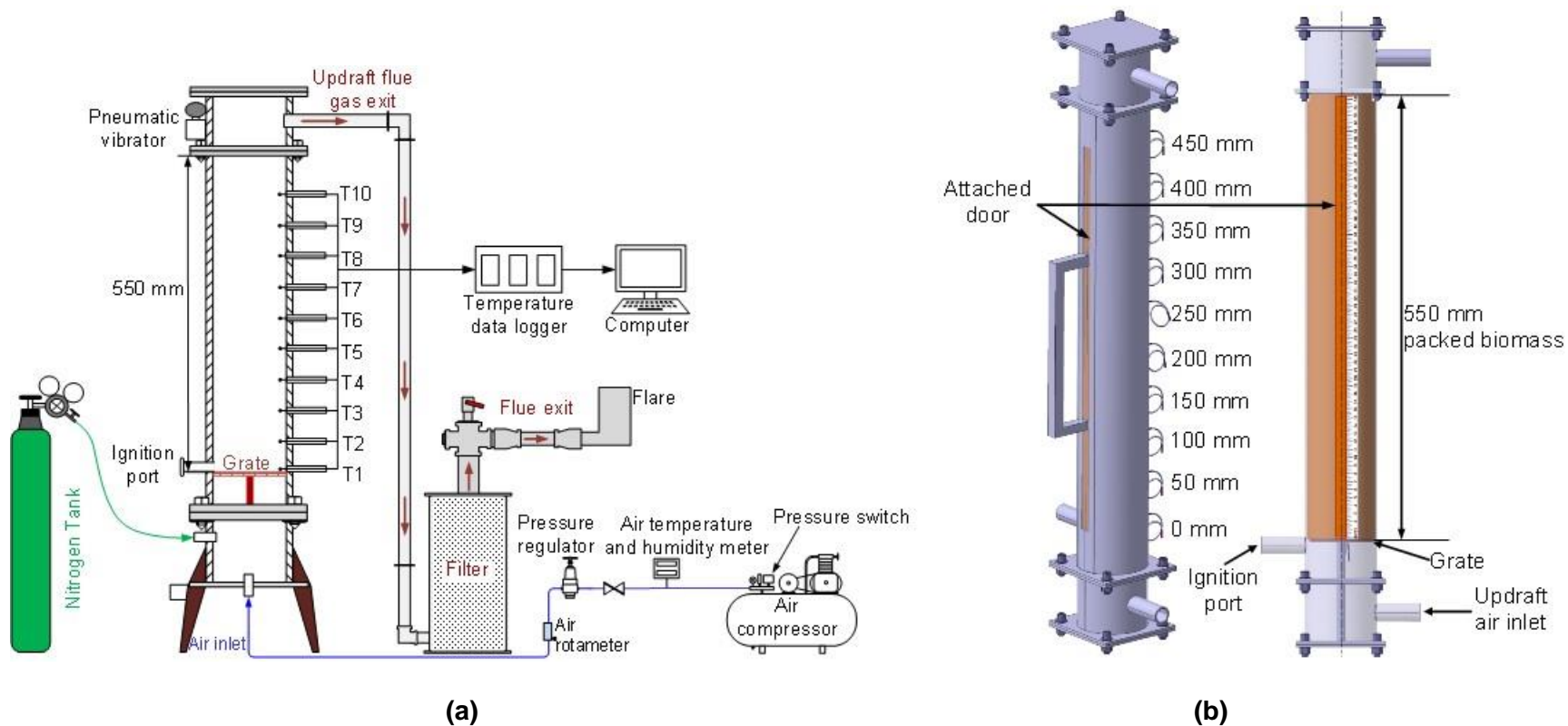


Fig. 1. (a) Experimental test rig diagram; (b) Gasification reactor

Repeatability

The reading temperature of every thermocouple at the selected three points in time for each air mass flux is selected (Fig. 2). The standard error was calculated as follows, (Kyu-Lee *et al.* 2015; Onthong and Charoensuk 2019),

$$SE = \frac{SD}{\sqrt{n}} \quad (2)$$

where SE is the standard error, SD is the standard deviation, and n is the number of samples.

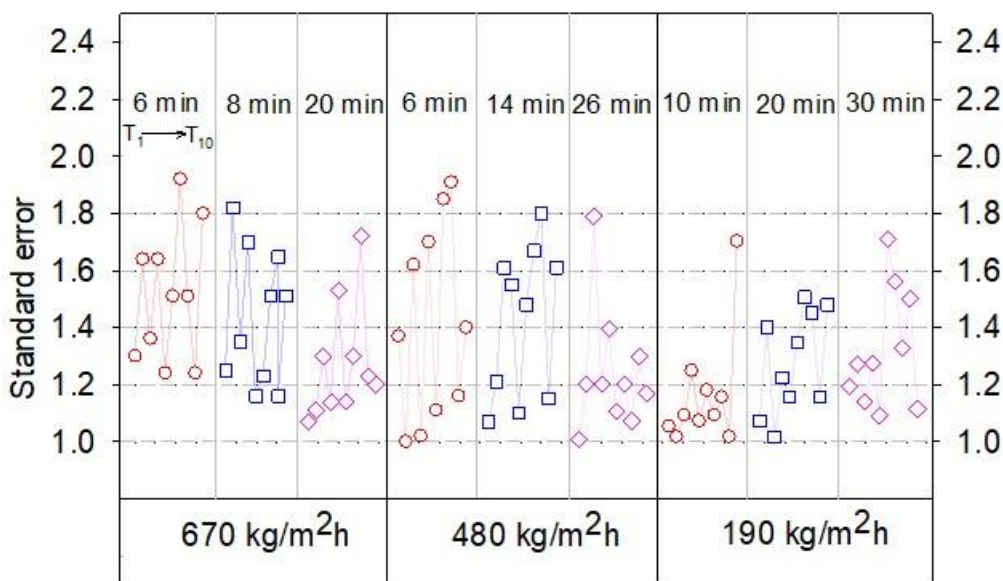


Fig. 2. Standard error

RESULTS AND DISCUSSION

General Phenomena in Thermochemical Treatment in an Updraft Reactor

Three different air mass fluxes of updraft thermochemical treatment were investigated. The temperature profile for all cases is comprised of the positive and negative gradient at every instant during the test period (Fig. 3). This coincides with other literature (Chin and Choi 2000; Hendriyana 2020). The different layer widths are identified by distinctive processes that appear along the treatment period. The oxidation zone (OZ) is located underneath. It is indicated by the positive temperature gradient. Above the oxidation zone, a negative temperature gradient is observed. This is due to heat loss of the hot-flowing gas to the fixed bed. Under the gasification regime, the fuel layer in a negative temperature gradient is comprised of a char gasification layer (reduction) followed by fresh fuel pyrolysis and a drying layer located on the top of the bed (Fig. 4). By contrast, in the char gasification or combustion regime, the fresh fuel pyrolysis and drying layer may not appear, as shown in Fig. 5 (Ryu *et al.* (2006).

For all experimental cases in this paper, the phenomena along the testing period can be divided into 2 phases: the combustion propagation phase (CP) and the fuel depleting phase (FD). In the CP period, the oxidation zone (OZ) is propagating upward from the fuel grate as indicated by the continuous expansion of the positive temperature gradient zone above the fuel grate, as shown in Fig. 6a. Temperature is increased with the increasing height, indicating that the combustion heat released occurs along this zone. The highest temperature at any instant in CP is located at the end of the OZ and is also increased with increasing time. After a certain period, the process will be changed from CP to FD. The point of time that the process switched from CP to FD is the peak temperature instant as shown in Fig. 6a. It can be noted by the occurrence of peak temperature at the end of the OZ. Finally the process will be changed to the FD phase which the kinetic activity is attenuated resulting in temperature decreasing at all locations in the reactor as shown in Fig. 6b.

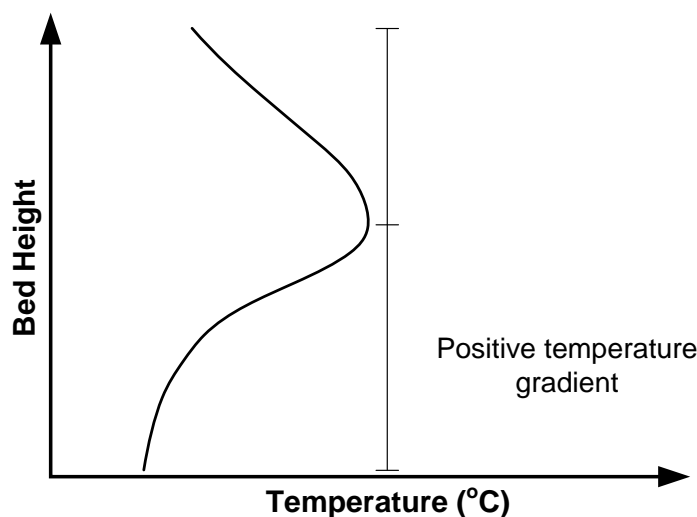


Fig. 3. Temperature profile of the updraft thermochemical treatment

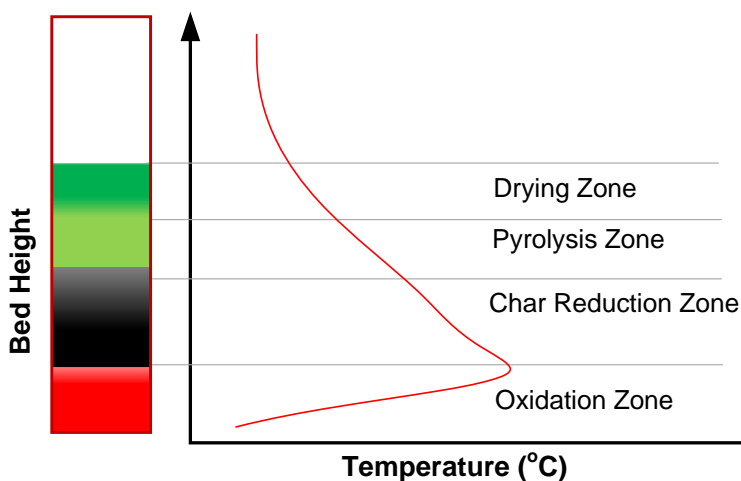


Fig. 4. Drying and pyrolysis layer above the oxidation and char reduction layer during updraft thermochemical treatment

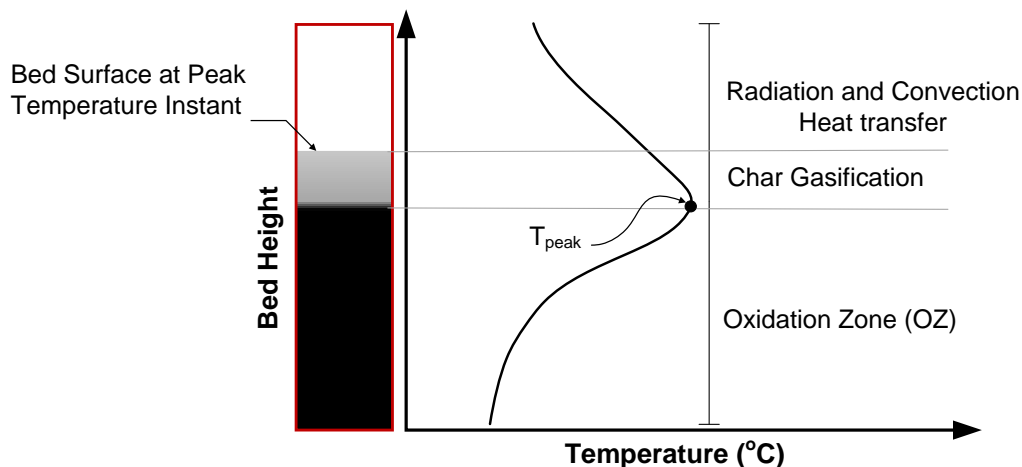


Fig. 5. Oxidation and char reduction layer during updraft thermochemical treatment

The CP period is started after igniting the flame at the ignition port above the fuel grate. A lot of steam was produced, as can be noted by the white smoke plume that flowed out from the top of the reactor. Steam is a non-combustible gas. It acts as a heat load, which reduced the combustion temperature. The OZ is expanding toward the top of the reactor. The intensity and the highest temperature at the end of OZ are increasing continuously. This is because the producer gas has higher energy intensity as steam, and heavy hydrocarbon contents were driven off during the beginning of the process. The bed height is decreased continuously as the size of the fuel particle is reduced. In the CP period, the temperature profile in the reactor can be divided into two zones, which are 1.) Positive temperature gradient along the axial direction from the fuel grate, which is the indication of OZ and 2.) Negative temperature gradient zone, which occurs above the OZ. The negative temperature gradient above OZ is due to heat expense in the gasification and drying of the fuel layer located above OZ. At a specific instant, as the thermochemical treatment is very dynamic, the gasification layer may include a char layer followed by a fresh biomass pyrolysis layer and the drying layer of fresh biomass on the top (Fig. 4), or it may be only char gasification layer above the OZ. The char gasification layer above the maximum temperature location is dominated by the presence of steam and CO_2 in the gas stream, which is the main content in the combustion products flowing from the OZ. They reacted with the carbon surface of the char above the OZ to convert CO_2 to combustible CO. The flowing gas will leave the top surface of the bed, which was significantly reduced in height due to the average fuel particle shrinkage during the thermochemical treatment process. The measured temperature above the top surface of the bed is decreased with increasing height. As the thermocouples in this zone receive the radiation heat transfer from the hot fuel bed below it and heat convection from the hot synthesis gas flowing upward from the fuel bed. The radiation intensity is decreased with increasing distance above the fuel bed. Therefore, the reading temperature of the thermocouples above the packed bed has an inverse variation with the distance above the bed surface.

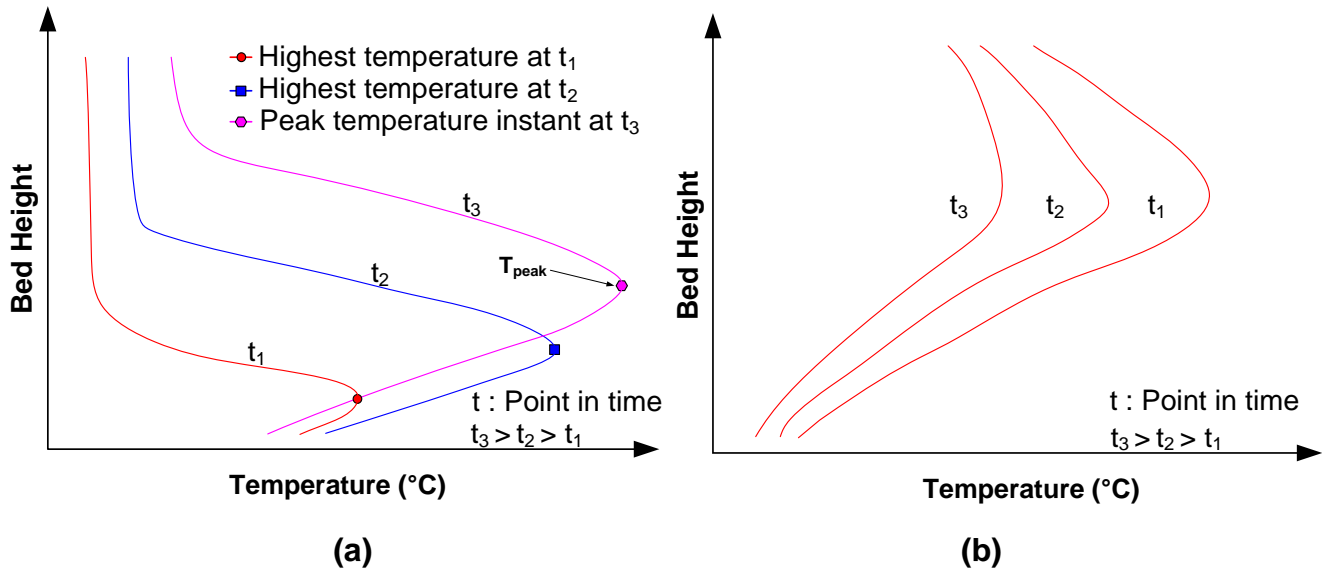


Fig. 6. (a) Temperature evolution at different time steps during the combustion propagation phase; (b) Temperature evolution at different time steps during the fuel depletion phase

Air Mass Flux of 670 kg/m²h

During the ignition period, the external burner is placed inside the ignition port, and all installed thermocouples are monitored every 30 seconds. Once any thermocouple reading is over 100 °C, the external burner is then removed and the ignition port is closed. At the same time, the stopwatch timer is started.

At the starting stopwatch timer, the temperature is increasing from the grate and reaches the maximum of 190 °C at T_2 . This indicates that the OZ is spread from the fuel grate to T_2 location. At the second minute, OZ is further expanded to T_4 (Fig. 7).

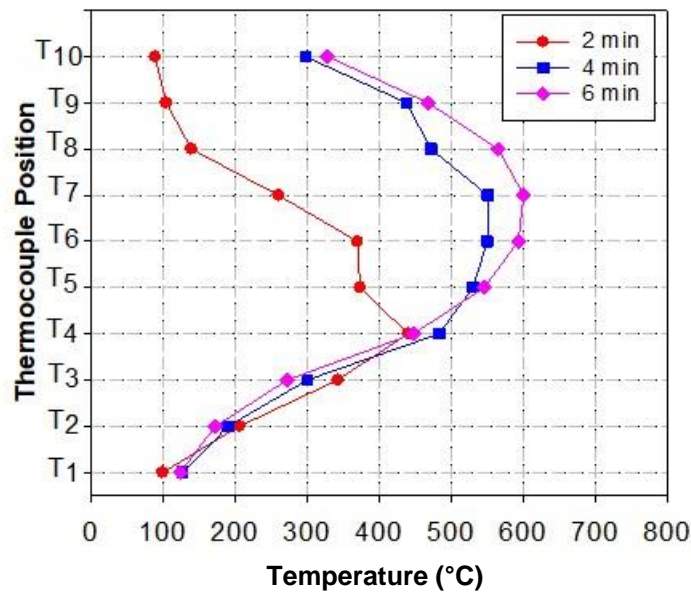


Fig. 7. Temperature evolution during the combustion propagation phase of air mass flux 670 kg/m²h.

The intensity of the combustion is also increased, as indicated by the increasing maximum temperature to 440 °C. At above T_4 , the temperature is decreased continuously from T_4 upward to the top of the reactor. The decrease in temperature is due to a combination of heat transfer from high-temperature gas flowing from the OZ to the low-temperature fuel and the endothermic reduction kinetic. At the sixth minute, the OZ covers the distance from the fuel grate to T_7 . The top surface of the fuel bed is located between T_7 and T_8 , as can be seen in Fig. 10 a. Therefore, all of the thermocouples above T_7 receive heat transfer from the flowing gas and the heat radiated from the fuel bed below. The decrease in the reading temperature of the thermocouples above T_7 with the increasing height is due to the radiation heat absorbed by each thermocouple, which will be decreased with the increasing distance above the top surface of the fuel bed. At the eighth minute, the largest temperature gradient within the OZ indicates the peak intensity of pyrolysis combustion activity. The peak temperature of 624 °C at T_7 is obtained at this instant (Fig. 8).

From the eighth minute onward, the temperature gradient of OZ is decreasing which indicates that the kinetic activities are attenuated. This corresponds with the forming ash around fuel particles, as can be seen in Fig. 10 c. The temperature of all locations decreased with increasing time, as shown in Fig 9. From Fig 10a, the packed bed color was homogeneously black at the sixth minute. The bed top surface height is around 340 mm from the grate. At peak temperature instant, the eighth minute, the bed height was reduced to 320 mm, as shown in Fig 10b. During FD, at twentieth minutes, the homogeneous ash layer around the fuel particles was observed along the bed. The bed height is reduced to 300 mm (Fig 10c). This indicates that the fuel conversion rate in the reactor was homogeneous throughout the entire process. This was because of the coordination between the widespread and low temperatures of the OZ and the bed movement from the particle shrinkage.

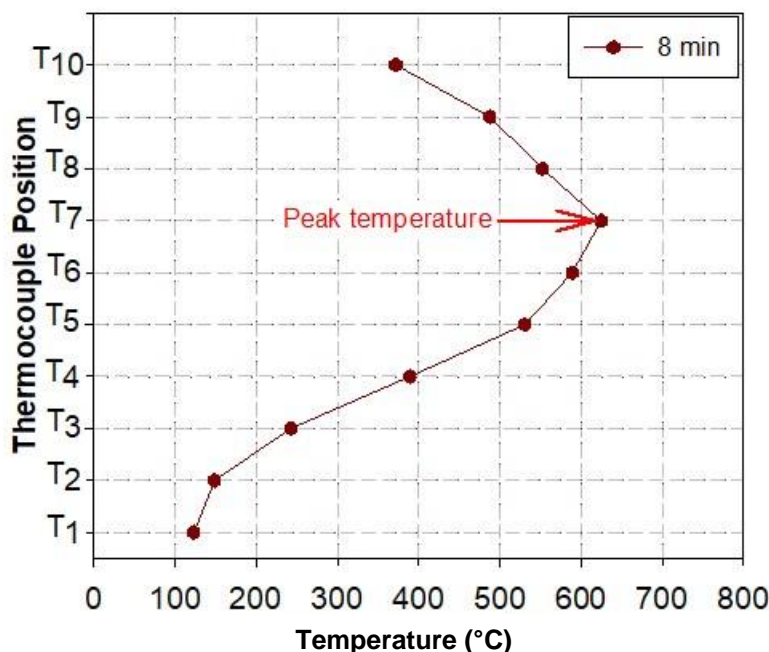


Fig. 8. Temperature distribution at peak temperature instant of air mass flux 670 kg/m²h

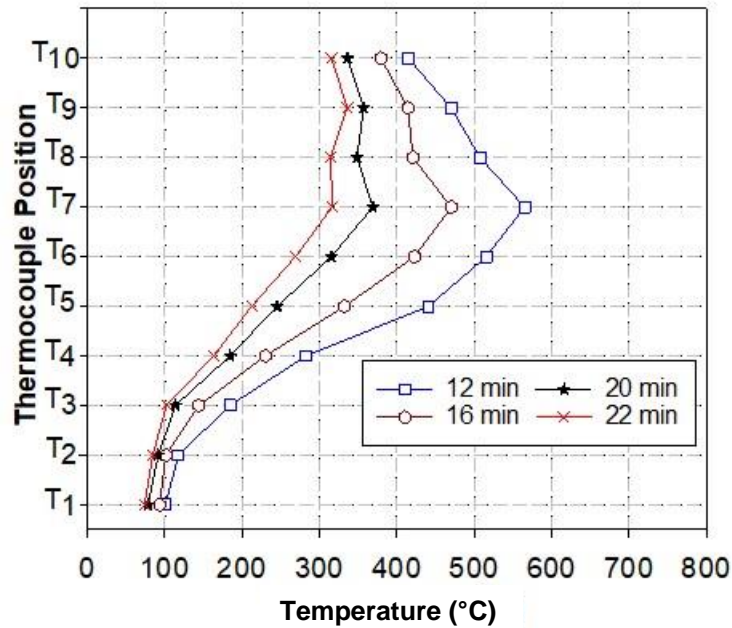


Fig. 9. Temperature evolution during the fuel depletion phase of air mass flux 670 kg/m²h

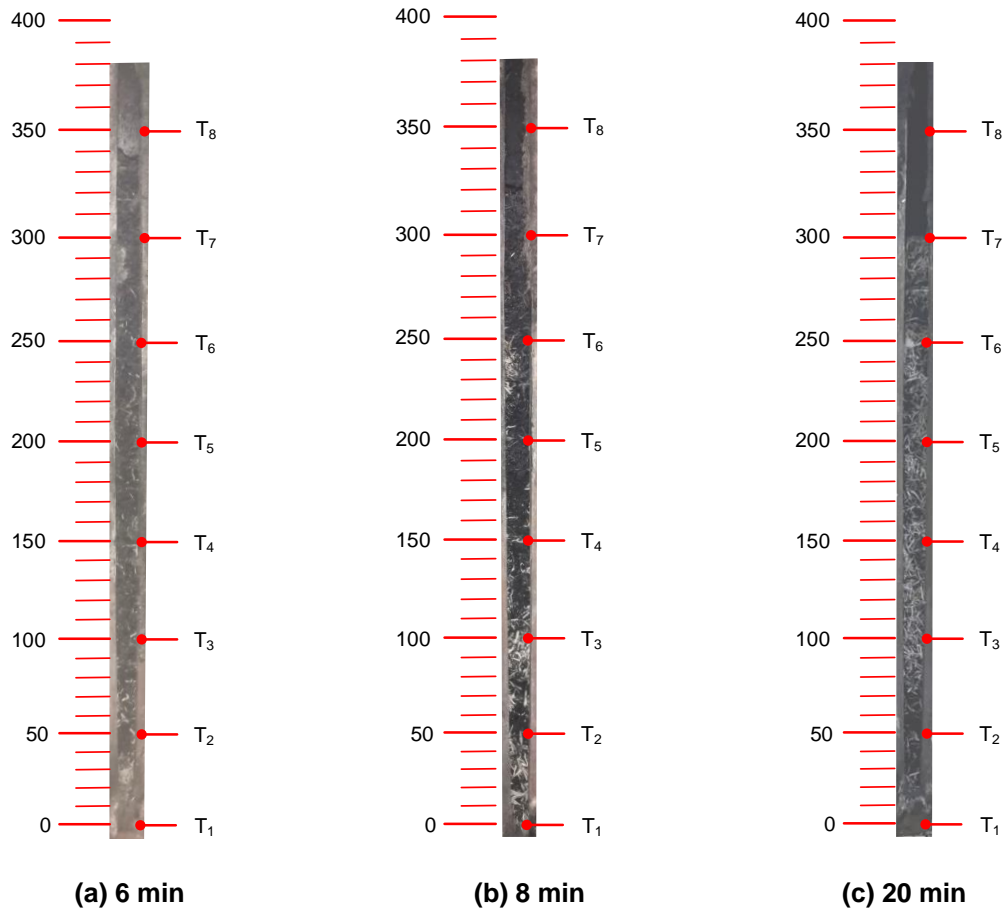


Fig. 10. Residual at the different instant of air mass flux 670 kg/m²h. (a) At 6th minute (during combustion propagation phase); (b) At 8th minute (peak temperature instant); (c) At 20th minute (during fuel depletion phase)

Air Mass Flux of 480 kg/m²h

For air mass flux 480 kg/m²h, the phenomena along the test are identical to air mass flux 670 kg/m²h. Starting from the CP period the OZ is expanding from the fuel grate, and the highest temperature is increased continuously with increasing time (Fig. 11). The OZ is expanding until it has covered the distance from the fuel grate to T₆ at the fourteenth minute. The peak temperature is 740 °C. The peak temperature and the temperature gradient of air mass flux 480 kg/m²h are considerably higher than of the air mass flux 670 kg/m²h during CP and the peak temperature instant (Figs. 8 and 12). At peak temperature instant, OZ is shorter than the air mass flux 670 kg/m²h because the combustion intensity is higher than the air mass flux 670 kg/m²h. As a result, all available oxygen was consumed within a shorter distance. It is evident that pyrolysis combustion of the air mass flux 670 kg/m²h has higher convection heat loss than this case. The convection heat loss will reduce the temperature and kinetic rate in the combustion zone. The reduction zone temperature gradient of the air mass flux 480 kg/m²h is also higher than the air mass flux 670 kg/m²h, as the higher reduction zone temperature promotes the endothermic reduction activity. The temperature evolution along FD is shown in Fig. 13.

From Fig. 14a, the packed bed color is homogeneously black at the sixth minute during CP. The positive temperature gradient is observed from the grate to 200 mm height (Fig. 11), which is an indication of the OZ. The distance from 200 mm to 360 mm is the char gasification (reduction) zone where the negative temperature gradient is revealed. At peak instant, as shown in Fig 14b, the white color is found from 160 mm to 260 mm height implying that the packed bed in this zone has been converted to ash. The high fuel conversion rate in this zone is due to the high temperature (hot pot) along OZ. The OZ covers the distance from the grate to 250 mm and the char reduction zone is starting from 250 mm to 315 mm. The ash layer further expands during FD as shown in Fig. 14c.

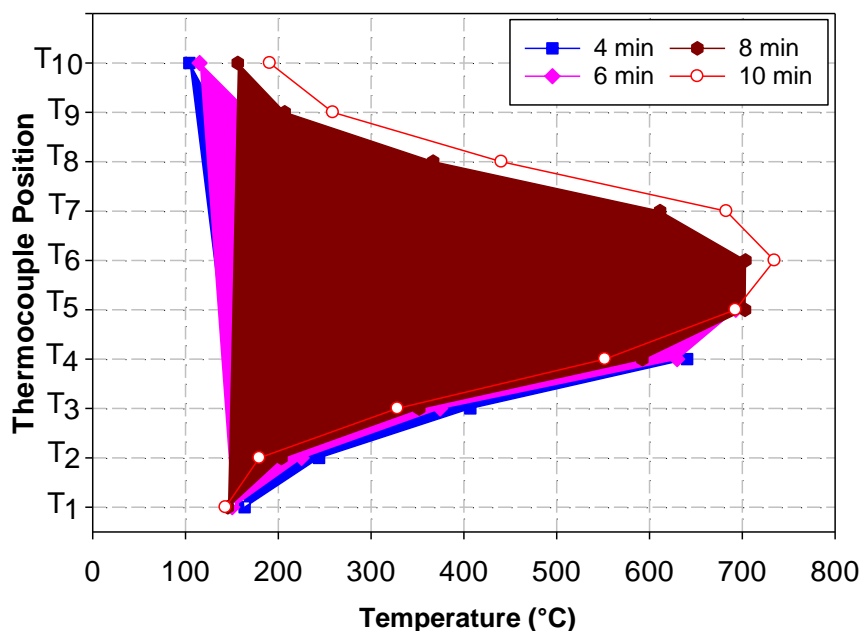


Fig. 11. Temperature evolution during the combustion propagation phase of air mass flux 480 kg/m²h

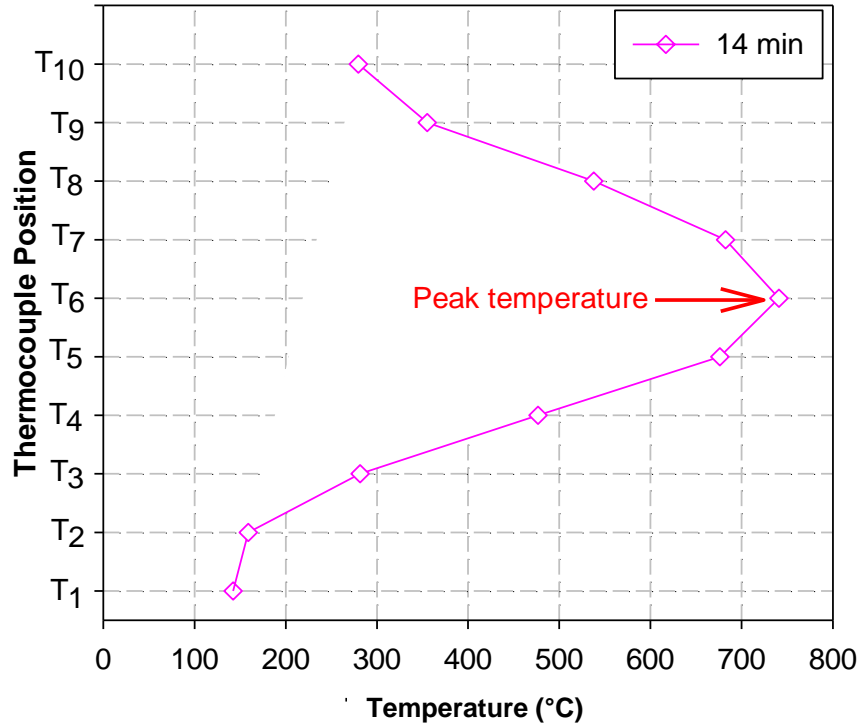


Fig. 12. Temperature distribution at peak temperature instant of air mass flux 480 kg/m²h

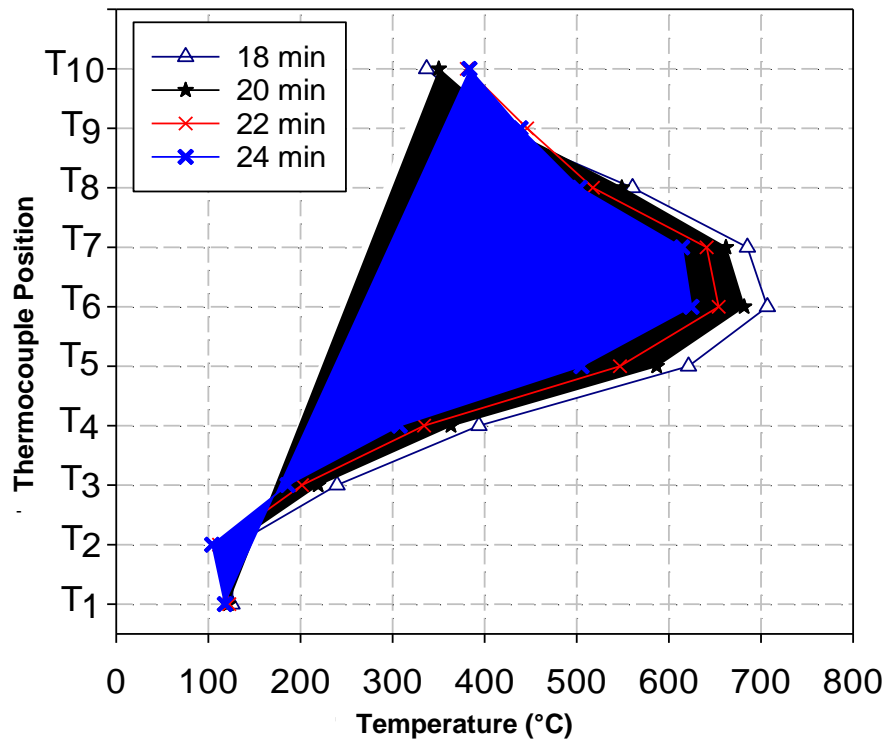


Fig. 13. Temperature evolution during the fuel depletion phase of air mass flux 480 kg/m²h

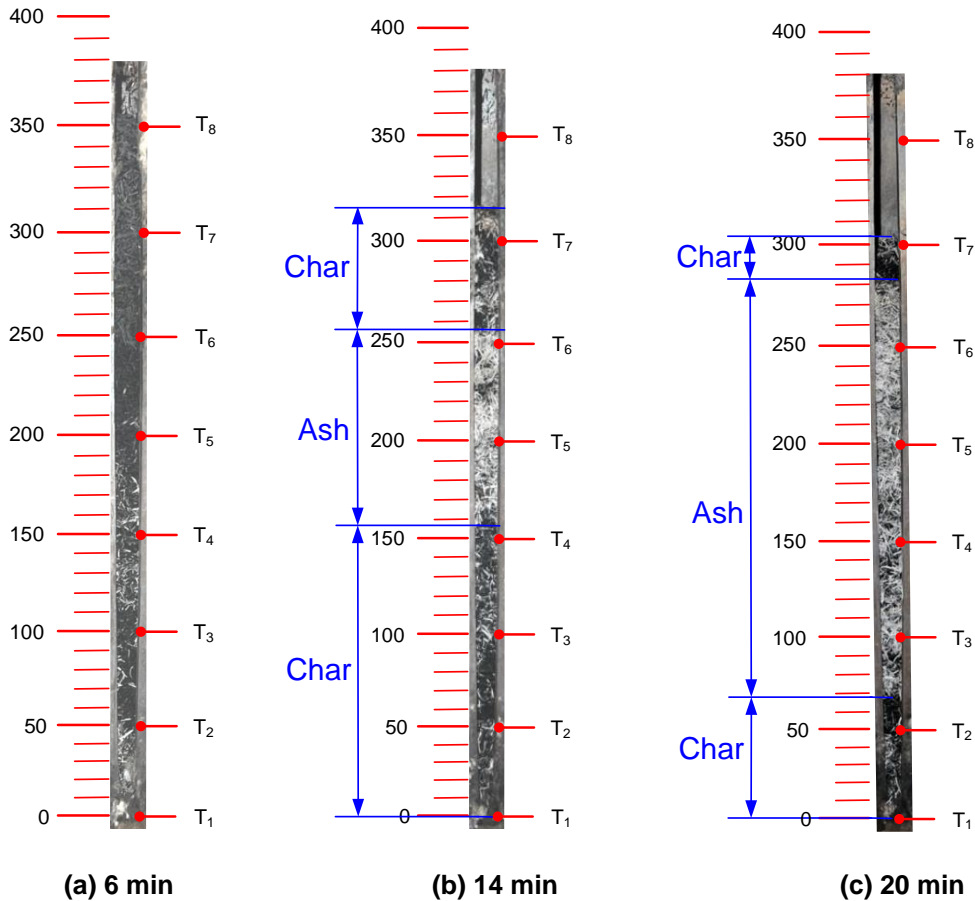


Fig. 14. Residual at different instant air mass flux $480 \text{ kg/m}^2\text{h}$. (a) At 6th minute (during combustion propagation phase); (b) At 14th minute (peak temperature instant); (c) At 20th minute (during fuel depletion phase)

Air Mass Flux of $190 \text{ kg/m}^2\text{h}$

For air mass flux of $190 \text{ kg/m}^2\text{h}$, the convection heat loss in OZ is at a minimum compared with the other two cases. The temperature and the temperature gradient in the OZ are comparable to the air mass flux $480 \text{ kg/m}^2\text{h}$. The peak temperature of $764 \text{ }^\circ\text{C}$ was obtained at T_6 , which is a little higher than the case air mass flux $480 \text{ kg/m}^2\text{h}$ (Figs. 12 and 16). At a certain time during CP, the large T_1 and T_2 temperature falling can be observed. This is because the fuel at that location has been converted to ash, as shown in Figs. 15 and 18 a. This eventually results in less oxygen used for combustion around T_1 and T_2 . As a consequence, there is leftover oxygen leaving the upper boundary of the OZ, which allows the upper OZ boundary to expand. The lower OZ boundary moved up from the grate because the fuel around T_1 and T_2 had been converted to ash and the upper OZ boundary expanded at nearly the same speed. This is analogous to the situation that OZ moved upward with nearly constant layer width. It can be depicted by Fig. 18 a, as the combustible char layer was clearly separated above the ash layer. The temperature above the fuel grate at the location of T_1 and T_2 of air mass flux $190 \text{ kg/m}^2\text{h}$ at the beginning of CP is considerably higher than the other two cases (Fig. 15) because of the low heat convection. This resulted in a higher combustion heat release rate and the higher fuel conversion rate, as the fuel in this region converted to ash quicker than in the rest two cases. The temperature evolution along FD is shown in Fig. 17.

The packed bed obviously shows three different layers at the twelfth minute in CP. The positive temperature gradient zone (Fig.15) at this instant indicates that the OZ covers the distance from the grate to 150 mm. The negative temperature gradient covers the distance from 150 mm toward the top (Fig.15). By mapping the temperature profile with the bed color in Fig. 18a, it is apparent that the char gasification zone (reduction) cover the distance from 150 mm to 315 mm. The green biomass pyrolysis and drying zone is above the char reduction zone from 315 mm to 350 mm. The ash layer covers the distance from the grate to 110 mm because of the hot spot zone above the grate during CP. At peak instant, twentieth minute, the ash layer is expanded to 200 mm length (Fig. 18b). The char reduction layer indicated by the negative temperature gradient (Fig. 15) covers the height from 250 mm to 345 mm. At minute 30, during FD, the ash layer is expanded to 270 mm. The 30 mm of small char reduction zone is seen above the ash layer, as shown in Fig. 18c.

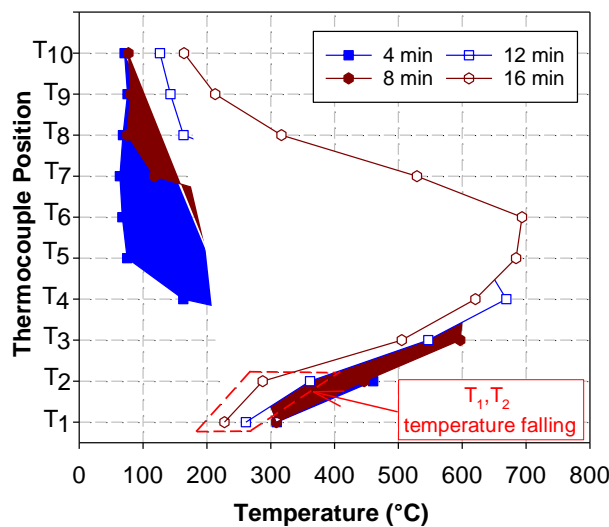


Fig. 15. Temperature evolution during combustion propagation phase of air mass flux 190 kg/m²h

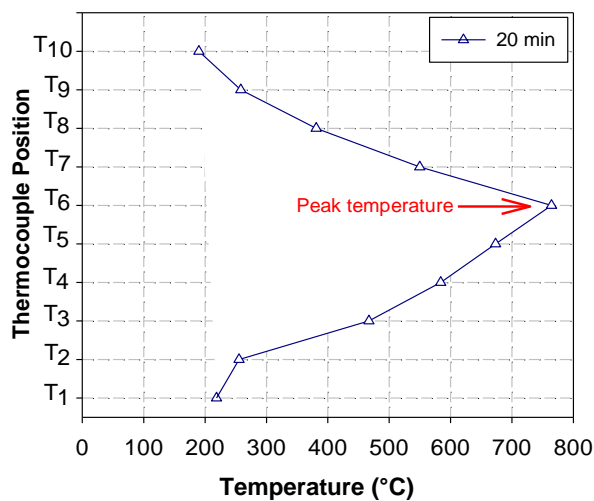


Fig. 16. Temperature distribution at peak temperature instant of air mass flux 190 kg/m²h

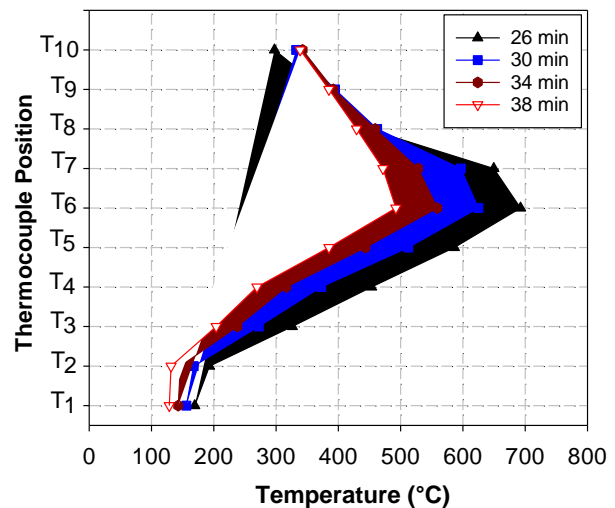


Fig. 17. Temperature evolution during the fuel depletion phase of air mass flux 190 kg/m²h

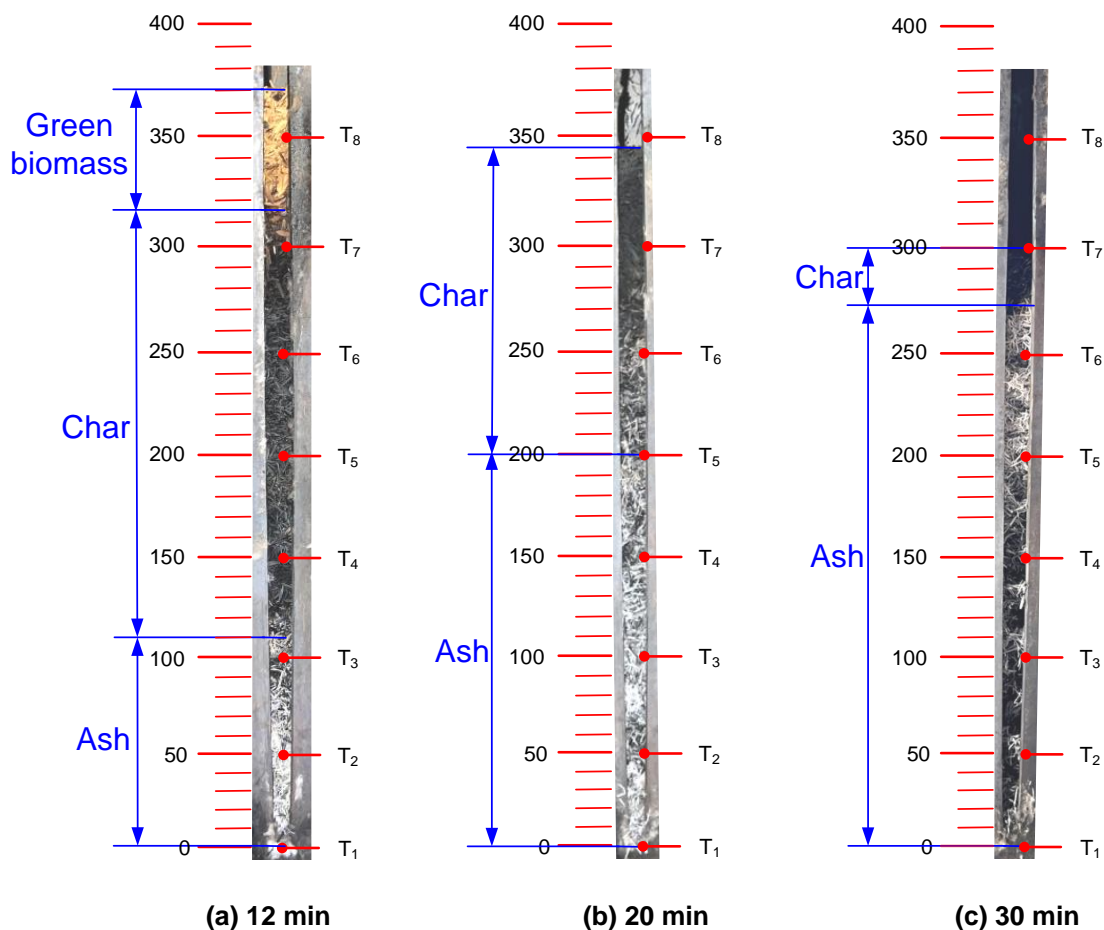


Fig. 18. Residual at different instant air mass flux $190 \text{ kg/m}^2\text{h}$. (a) At 12th minute (during combustion propagation phase); (b) At 20th minute (peak temperature instant); (c) At 30th minute (during fuel depletion phase)

Fuel Residual Analysis

For air mass flux $670 \text{ kg/m}^2\text{h}$, during CP, all fresh fuel along the reactor height has been converted to char at the sixth minute (Fig. 10 a). The residual at any specified instant appears as a homogeneous black surface comprising the entire reactor height, as shown in Figs. 10a and 10b. This indicates that the heat transfer to the fuel bed along different layers is evenly distributed during the entire process. Therefore, the average fuel conversion rate is not much different along the reactor height. None of the hot spots develop in the OZ due to high convection loss and high heat transfer rate from the OZ to the above fuel layer compared with the other two cases.

For air mass flux $480 \text{ kg/m}^2\text{h}$, at peak temperature instant, it is evident that the residual layer between T_5 and T_6 has been converted to ash (Fig. 14b) because the hot spot temperature is located around this location from the beginning of the test. The peak temperature is higher than in the case of air mass flux $680 \text{ kg/m}^2\text{h}$ because of the lower convection heat transfer. The final residual showed the black char above the fuel grate (around T_1 and T_2) and also at the T_7 (Fig. 14c), while the fuel has been converted to ash within the boundary from T_3 to T_6 . This is evidence that the fuel conversion rate is much faster around the hot spot zone than in the other location.

For air mass flux $190 \text{ kg/m}^2\text{h}$, during CP the large difference in fuel conversion rate along the axial distance of the reactor was revealed. The fuel was completely converted to ash near and underneath where the high hot spot temperature was situated in the OZ during the beginning of CP. The convection heat transfer in an upward direction to the fresh fuel above OZ is considerably less than in the other two cases.

CONCLUSIONS

1. An experimental investigation of updraft gasification has been performed. The test rig was equipped with a special attached door that will open at a specific time step. Before opening the attached door, airflow is cut off and nitrogen is made to flow through the bed immediately to ensure that the kinetic inside the reactor is instantly halted. Then water is sprayed around the reactor surface to allow fast bed cooling. This unique feature will allow investigators to obtain information on the packed bed color variation along the different heights of the reactor that evolves at different points in time. The packed bed color variation can be served as supplementary information to identify the state of fuel conversion (fresh biomass, char, ash). The fuel composition analysis at different heights of the packed bed could be performed to increase the investigation's accuracy. The analysis is focused on the temperature dynamics with the packed bed color variation at each time step. The investigation has been conducted for three different supply air mass fluxes, which were 670 , 480 , and $190 \text{ kg/m}^2\text{h}$, corresponding with the equivalence ratio of 0.27 , 0.33 , and 0.20 , respectively.
2. General behavior was identical for all three supply air mass fluxes. It comprised the combustion propagation phase (CP) during the first phase, followed by the fuel depletion phase (FD). In the combustion propagation phase (CP), the oxidation zone (OZ) was expanding continuously. The highest temperature is increased with increasing time. The air mass flux $670 \text{ kg/m}^2\text{h}$ had the lowest peak temperature of 624°C because of the high convection. The lowest temperature gradient was also observed all over the heat-affected zone. The high peak temperature was observed in the case $480 \text{ kg/m}^2\text{h}$ and $190 \text{ kg/m}^2\text{h}$ which were 740°C and 764°C , respectively. This was due to the low convection loss in the oxidation zone.
3. The homogeneous fuel conversion along the packed bed was observed for air mass flux $670 \text{ kg/m}^2\text{h}$ due to high convection heat transport from the OZ to all locations of the packed bed. For air mass flux of $480 \text{ kg/m}^2\text{h}$, the high fuel conversion was found around the middle of the reactor as the ash layer appeared from the bed height of 160 mm to 260 mm . This coincides with the peak temperature location. For an air mass flux of $190 \text{ kg/m}^2\text{h}$, there is an obvious hot spot found around the bottom of the bed at the very first period of the process. The fuel at the grate quickly converted to ash. The 110 mm of ash layer was revealed at the twelfth minute during the combustion propagation phase. The ash layer was expanded to cover the distance from the grate to 200 mm height at the peak instant.

ACKNOWLEDGMENTS

This research was funded by King Mongkut's University of Technology North Bangkok, Contract no. KMUTNB-65-NEW-12

REFERENCES CITED

- Basu, P. (2010). *Biomass Gasification and Pyrolysis: Practical Design and Theory*, Academic Press, New York, NY.
- Blasi, C. D. (2000). "Dynamic behaviour of stratified downdraft gasifiers," *Chemical Engineering Science* 55, 2931-2944.
- Friberg, R., and Blasiak, W. (2002). "Measurements of mass flux and stoichiometry of conversion gas from three different wood fuels as function of volume flux of primary air in packed-bed combustion," *Biomass and Bioenergy* 23(3), 189-208. DOI: 10.1016/S0961-9534(02)00048-X
- Hendriyana. (2020). "Effect of equivalence ratio on the rice husk gasification performance using updraft gasifier with air suction mode," *Jurnal Bahan Alam Terbarukan* 9(1), 30-35. DOI :10.15294/jbat.v9i1.23527
- Jancauskas, A., and Buinevicius, K. (2021). "Combination of primary measures on flue gas emissions in grate-firing biofuel boiler," *Energies* 14, DOI: 10.3390/en14040793
- Kim, M., Lee, Y., Park, J., Ryu, C., and Ohm, T. I. (2016). "Partial oxidation of sewage sludge briquettes in an updraft fixed bed," *Waste Management* 49, 204-211. DOI: 10.1016/j.wasman.2016.01.040
- Madhiyanon, T., Sathitruangsak, P., Sungworagarn, S., and Udomman, T. (2020). "Investigation of rice-straw-ash fouling/slagging and countermeasures using supplementary additives and co-firing with Si-Al-rich coal in a pilot-scale grate-fired combustor," *Journal of the Energy Institute* 93(5), 1848-1867. DOI: 10.1016/j.joei.2020.04.001
- Mehta, Y., and Richards, C. (2017). "Gasification performance of a top-lit updraft cook stove," *Energies* 10, DOI: 10.3390/en10101529
- Onthong, K., and Charoensuk, J. (2019). "A new method for zone development observation for updraft rice husk gasification," *BioResources* 14(3), 5080-5096. DOI: 10.15376/biores.14.3.5080-5096
- Rashidian, B., Al-Abdeli, Y. M., Patino, D., Guzzomi, F. G., and Yeoh, H. G. (2016). "Effect of freeboard deflectors in the fixed bed combustion of biomass," *Applied Thermal Engineering* 103, 543-552. DOI: 10.1016/j.applthermaleng.2016.04.140
- Reed, T. B., and Das, A. (1988). *Handbook of Biomass Downdraft Gasifier Engine Systems*, Solar Energy Research Institute, Golden, CO, USA.
- Ryu, C., Yang, Y. B., Khor, A., Yates, E. N., Sharifi, V. N., and Swithenbank, J. (2006). "Effect of fuel properties in biomass combustion: Part I. Experiments-fuel type, equivalence ratio and particle size," *Fuel* 85(7-8), 1039-1046. DOI: 10.1016/j.fuel.2005.09.019
- Ryu, C., Phan, A. N., Sharifi, V. N., and Swithenbank, J. (2007). "Co-combustion of textile residues with cardboard and waste wood in a packed bed," *Experimental Thermal and Fluid Science* 32, 450-458. DOI: 10.1016/j.expthermflusci.2007.05.008
- Sharma, P., Gupta, B., Pandey, M., Bisen, K.S., and Baredar, P. (2021). "Downdraft biomass gasification: A review on concepts, designs analysis, modelling and recent

- advances,” *Materials Today: Proceedings* 46(11), 5333-5341. DOI: 10.1016/j.matpr.2020.08.789
- Shin, D., and Choi, S. (2000). “The combustion of simulated waste particles in a fixed bed,” *Combustion and Flame* 121(1-2), 167-180. DOI: 10.1016/S0010-2180(99)00124-8
- Susastriawan, A. A. P., Purwanto, Y., Sidharta, B. W., Wahyu, G., Trisna, T., and Setiawan, R. A. (2021). “Producer gas stove: Design, fabrication, and evaluation of thermal performance,” *Journal of King Saud University - Engineering Sciences*, DOI: 10.1016/j.jksues.2021.10.009
- Susastriawan, A. A. P., Saptoadi, H., and Purnomo. (2018). “Effect of tuyer distance above grate on propagation front and performance of downdraft gasifier with feedstock of rice husk,” *Renewable Energy* 134, 1034-1041. DOI: 10.1016/j.renene.2018.11.110
- Tanui, J. K., Kionia, P. N., Mirreb, T., and Nowitzkib, M. (2018). “The effect of carbon dioxide on flame propagation speed of wood combustion in a fixed bed under oxy-fuel conditions,” *Fuel Processing Technology* 179, 285-295. DOI: 10.1016/j.fuproc.2018.07.010
- Varunkumar, S., Rajan, N. K. S. and Mukunda, H. (2013). “Universal flame propagation behavior in packed bed of biomass,” *Combustion Science and Technology* 185(8), 1241-1260. DOI: 10.1080/00102202.2013.782297
- Voss, S., Mendes, M. A. A., Pereira, J. M. C., Ray, S., Pereira, J. C. F., and Trimis, D. (2013). “Investigation on the thermal flame thickness for lean premixed combustion of low calorific H₂/CO mixtures within porous inert media,” *Proceedings of the Combustion Institute* 34, 3335-3342. DOI: 10.1016/j.proci.2012.06.044
- Wasinarom, K., Charoensuk, J., and Lilavivat V. (2019). “Non-equilibrium numerical modeling for combustion of LPG within porous media,” *International Journal of Heat and Mass Transfer* 143, DOI: 10.1016/j.ijheatmasstransfer.2019.118551
- Wasinarom, K., Sungworagarn, S., Sathitruangsak, P., and Onthong, K. (2021). “Formation of multiple combustion fronts in an imbert downdraft gasification reactor,” *E3S Web of Conferences* 302, DOI: 10.1051/e3sconf/202130201007
- Yang, Y. B., Ryu, C., Khor, A., Sharifi, V. N., and Swithenbank, J. (2005). “Fuel size effect on pinewood combustion in a packed bed,” *Fuel* 84, 2026-2038. DOI: 10.1016/j.fuel.2005.04.022

Article submitted: January 2, 2023; Peer review completed: January 21, 2023; Revised version received: February 23, 2023; Accepted: March 20, 2023; Published: March 27, 2023.

DOI: 10.15376/biores.18.2.3452-3470